Maturity Cycles in Implied Volatility

Jean-Pierre Fouque* George Papanicolaou† Ronnie Sircar‡
Knut Solna§

August 14, 2002

Abstract

The skew effect in market implied volatility can be reproduced by option pricing theory based on stochastic volatility models for the price of the underlying asset. Here we study the performance of the calibration of the S&P 500 implied volatility surface using the asymptotic pricing theory under fast mean-reverting stochastic volatility described in [6]. The time-variation of the fitted skew-slope parameter shows a periodic behaviour that depends on the option *maturity dates* in the future, which are known in advance. By extending the mathematical analysis to incorporate model parameters which are time-varying, we show this behaviour can be explained in a manner consistent with a large model class for the underlying price dynamics with time-periodic volatility coefficients.

Contents

*Department of Mathematics, NC State University, Raleigh NC 27695-8205, *fouque@math.ncsu.edu.* Work partially supported by NSF grant DMS-0071744.

†Department of Mathematics, Stanford University, Stanford CA 94305, *papanico@math.stanford.edu.*

‡Department of Operations Research & Financial Engineering, Princeton University, E-Quad, Princeton, NJ 08544, *sircar@princeton.edu.* Work supported by NSF grant DMS-0090067. We are grateful to Peter Thurston for research assistance.

§Department of Mathematics, University of California, Irvine CA 92697, *ksolna@math.uci.edu.*

1 Introduction

The problem of calibrating market implied volatilities is often described as having three dimensions : K, T and t. The first refers to finding a model (or class of models) for the underlying asset dynamics that captures the variation of implied volatilities as functions of strike (the smile, or skew in equities and indices); the second refers to the term-structure, or variation over maturities of the options; the small t refers to the variation of the surface over time: if this is not captured well by the model, it leads to instability over time of calibrated parameters. Obtaining stability is crucial for pricing path-dependent options and for hedging.

The first problem can be addressed by many types of models that have fat, and possibly asymmetric tails in returns distributions, for example stochastic volatility models or models with jumps. The other two problems are more challenging. Many approaches deal with these problems successively, trying to obtain a tight in-sample fit[1] by allowing many degrees of freedom, without regard to the underlying price dynamics. The cost is poor stability properties. In previous work [6], we have studied an approach that approximately captures the K and T problems and has fairly good stability properties. We discuss those issues in detail in this work, and introduce a simple extension which improves its performance in all three dimensions.

The calibration procedure we propose here is simply to fit the surface to a straight line in a composite variable (called the log-moneyness-to-*effective*-time-to-maturity), but despite its simplicity, it is consistent with (and derived from) popular mean-reverting models of random volatility, and their associated *no arbitrage* restrictions. When applied to S&P 500 data (across both strikes *and* maturities), the in-sample fit to the surface is fairly good

[1] By in-sample fit, we mean how well the model fits the data from which it is calibrated.

for maturities on the order of a few months, as shown, for example, in Figure 10. More importantly the variation of the estimated parameters over time is relatively small, as shown in Figure 12, indicating that the procedure (and underlying models) have good stability properties.

The fast mean-reversion (FMR) asymptotic theory developed in [6] is designed to capture some of the important effects that fluctuations in the volatility have on derivative prices. In particular it shows how the implied volatility is affected. In the simplest case it suggests to fit the observed implied volatility surface I to an affine function of the log-moneyness-to-maturity ratio (LMMR):

$$\begin{aligned} I &= a \times \mathrm{LMMR} + b, \\ \mathrm{LMMR} &= \frac{\log(K/S)}{T-t}, \end{aligned} \tag{1}$$

and thereby to estimate two group market parameters a (the slope) and b (the intercept). Here K is strike price, T is expiration date and S is the asset price or index level at time t.

This approximation for the implied volatility surface arises from the following class of stochastic volatility models for the stock price (S_t) and the volatility driving process (Y_t):

$$dS_t = \mu S_t\, dt + f(Y_t) S_t\, dW_t,$$

where (W_t) is a standard Brownian motion and (Y_t) is an ergodic (or "mean-reverting") Markov Itô process with a unique invariant distribution, driven by a second Brownian motion $(\hat{Z}_t)$ that is correlated with (W_t). The function f is positive, bounded above and away from zero.

1.1 Volatility Mean-Reversion

To fix ideas and to allow us to refer to decorrelation speeds and rates of mean-reversion in terms of specific parameters, we shall write (Y_t) as an Ornstein-Uhlenbeck (OU) process:

$$dY_t = \alpha(m - Y_t)\, dt + \nu\sqrt{2\alpha}\, d\hat{Z}_t, \tag{2}$$

where (W_t) and $(\hat{Z}_t)$ have instantaneous correlation ρ, with $|\rho| < 1$.

The process Y has a unique invariant distribution, namely $\mathcal{N}(m, \nu^2)$, and is a simple building-block for a large class of stochastic volatility models described by the choice of $f(\cdot)$. The parameter α characterizes the *speed* of the process. It measures the exponential decorrelation rate, and ν characterizes the typical *size* of fluctuations of the volatility driving process.

The formula (1) is accurate in the regime of fast decorrelation (α large) of the process (Y_t). The precise order of this approximation is obtained in [5].

1.2 Fast Mean-Reversion of Volatility

In [4], we studied high-frequency S&P 500 data over the period of one year. The major difficulty with high-frequency data is pronounced intraday phenomena associated with microscopic trading patterns as described, for example, in [3]. In [4], it was shown how this

'periodic day effect' impacted the variogram and spectral methods used to analyze the data, and therefore how to account for it.

The result was, for the S&P 500 data examined, the presence of a *fast* volatility factor with rate of mean reversion $\alpha \sim 130 - 230$ (in annualized units). Note that the rate of mean-reversion of the unobserved volatility factor is extremely difficult to estimate *precisely*, hence the large range. This was confirmed from tests on simulated data.

Many empirical studies have looked at low-frequency (daily) data, with the data necessarily ranging over a period of years, and they have found a *low* rate of volatility mean-reversion. This does not contradict the empirical finding described above: analyzing data at lower frequencies over longer time periods would primarily pick up a slower time-scale of fluctuation and could not identify scales below the sampling frequency. At present, we will concentrate on the fast factor only and discuss extensions to include a slower factor in Section 6. We argue that this performs well empirically for S&P 500 options of up to the order of a few months from maturity, but that the extra factor extension is needed for longer options.

Another recent empirical study [2], this time of exchange rate dynamics, finds "the evidence points strongly toward two-factor [volatility] models with one highly persistent factor and one quickly mean-reverting factor". To pull one estimate from their Table VI, they find the rate of mean-reversion of the fast volatility factor for the US Dollar-Deutsche Mark exchange rate to be $\alpha = 237.5$ (in annualized units). For the other four exchange rates they also look at, the order of magnitude of this parameter is the same (hundreds).

1.3 Goal

The purpose of this article is to study the performance of (1) when fitted to real data and to introduce an extended theory with time-dependent periodic parameters that picks up a significant feature of the data. The criteria used here are

- goodness of the in-sample fit;
- stability of fitted parameters over time.

One common observation we would like to understand is:

For fixed $K \neq S$, the term-structure (variation with time-to-maturity $T - t$) is not like $(T-t)^{-1}$ but more like $(T-t)^{-1/2}$:

$$I \sim \frac{1}{\sqrt{T-t}}. \tag{3}$$

In Section 2, we look at the daily slope and intercept estimates (a and b in (1)) from S&P 500 index option implied volatilities. These shed some light on the previous observation. More strikingly, they identify a systematic almost-periodic behaviour in the slope of the skew (looked at as a function of LMMR). This is shown in Figure 3. *We argue that just as implied volatility is a convenient transformation through which to observe deviations of options prices from the Black-Scholes theory, the LMMR representation is useful for picking out secondary phenomena, once the basic skew shape has been captured by a stochastic volatility theory.*

We claim that the near-periodicity in the skew slope stems from option expiration dates, around the third Friday of each month. An examination of the calendar shows that the

"jumps" in the fitted skew slope, when the cycle returns to the beginning (it is not continuous), coincides with the closest-to-maturity options disappearing from the data. The fact that some options are expiring has a mild "feedback effect" on the entire options market (with the common underlying), probably through the volatility of the underlying itself.

Rather than proposing a mechanism that might explain this, we model in Section 4 the empirical observation directly through a periodic variation in the *speed* of the process driving volatility. We present the proof of the adjusted asymptotic theory in the general case of time-dependent volatility parameters in Section 3, and then specialize to only the speed being time-dependent in Section 4. The obstacle that makes the mathematical analysis interesting is the nonsmoothness of the call (or put) option payoff. It requires a carefully-chosen regularization that allows use of the explicit Black-Scholes formula to quantify the rate of blow-up of higher order derivatives with respect to the stock variable, that are needed in the proof.

The asymptotic analysis shows that the formula (1) prevails under periodic variation in the parameters for the underlying price dynamics when we are far from maturity, but is modified when we get closer to maturity. This correction shows how the seemingly contradictory observations (1) and (3) can be bridged and explained in terms of a transition in between these two regimes.

Finally, in Section 5, we parametrize the near-periodic behaviour of the speed function and fit to data, leading to improved stability of the fitted parameters over time. We present the results from S&P 500 implied volatilities from January 2000 through March 2001, and remark that similar results were also obtained using the 1993 S&P 500 dataset used in [1].

2 Fit of Implied Volatilities to LMMR Formula

2.1 Dataset

Our dataset contains implied volatilities from closing S&P 500 European option prices from January 2000 through March 2001. On each day, there are typically about 70 strikes (ranging over approximately 35% to 145% moneyness) and 7 maturities ($1, 2, 3, 6, 12, 15$ and 18 months). Throughout the empirical analysis, we will restrict ourselves to options *between* 70% *and* 102% *moneyness* so as to be on the safe side of liquidity issues. For much of the analysis we shall also restrict ourselves to options with three months or less to maturity since we are concerned with improving the fit to the shortest-dated options. We discuss an extension which could lead to improved capturing of the longer-term implied volatilities in the conclusions.

2.2 LMMR Fit across Maturities up to one year

On a typical day if we plot implied volatility as a function of LMMR including options with at least two and at most 93 days (three months) to maturity, we see an array of distinct *diverging* strands corresponding to each maturity, as in Figure 1. This picture tells us that the sharper the (negative) slope of the implied volatility (as a function of LMMR) on this plot, the *longer* the maturity. (Typically, we think of S&P 500 implied volatilities as a function of strike becoming sharper for *shorter* maturities, as shown in Figure 2, so the adjustment by

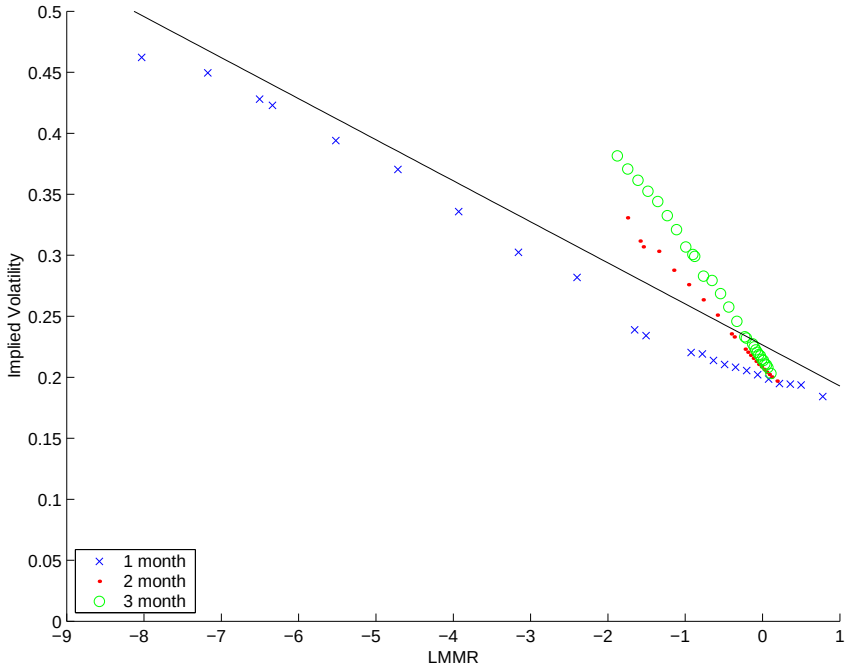

Figure 1: *Implied volatility as a function of LMMR on January 12, 2000, for options with at least two and at most* 93 *days to maturity. The one month options expire in January, the two month in February, and so on. Notice the distinct strands for each maturity, in particular the large gap between the one-month and two-month implied volatilities. The solid line is the least-squares straight line fit over all these maturities and strikes at once.*

the time-to-maturity has over-corrected for this feature). In fact if we were to fit a straight line to each strand separately, the fits would be good, but there would be a different slope estimate for each maturity. The LMMR theory can be used satisfactorily in this way, but we would like to incorporate term-structure effects in observed implied volatilities in the way we use stochastic volatility models (that is, to capture the T dimension of the problem discussed in the introduction).

We see that if we try and fit across a range of maturities, the in-sample fit is not very good (see the solid line in Figure 1).

More strikingly, if we look at the daily variation of the fitted parameters, as in Figure 3, there is a pronounced near-periodic repetition in the LMMR skew slope a, the period being on the order of twenty trading days. Further, there is a clear stratification, meaning the slopes jump down once each period.

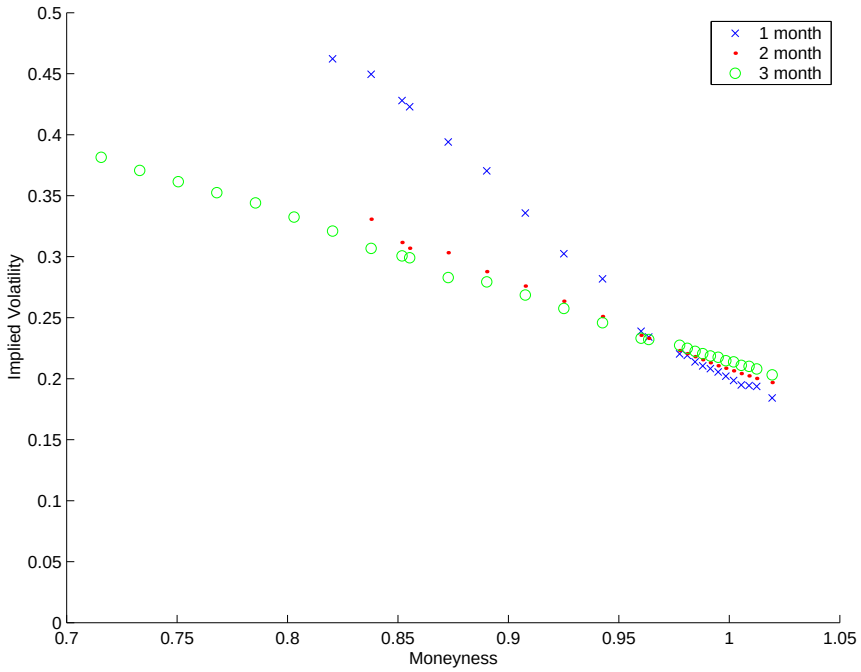

Figure 2: *Implied volatility as a function of moneyness on January 12, 2000, for options with at least two days and at most three months to maturity.*

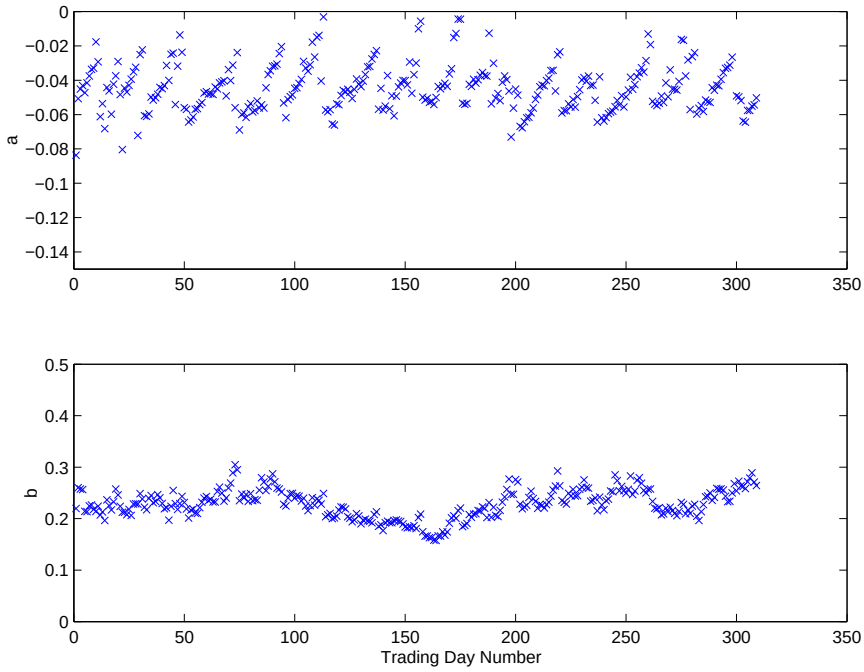

Figure 3: *Daily fitted LMMR parameters for options with at least* 2 *and at most* 93 *days to maturity, showing the periodicity corresponding to the monthly maturity cycle. Statistics: Mean* $(a) = -0.0444$, *Std* $(a) = 0.0137$; *Mean* $(b) = 0.2288$, *Std* $(b) = 0.0278$.

2.3 Examination of the Breaks

To try to understand what causes the sudden but regular discontinuities in the a's, we look at in-sample fits on days before and after a jump in Figure 3. It is clear from Figure 3 that the breaks are roughly a month apart, and a comparison with the calendar shows they occur exactly when the shortest maturity options included in the fit disappear (in Figure 3, two days before the third Friday of each month, for example).

Figure 4 shows fits on the last day of one stratum and the first day of the next. The disappearance of the shortest option has sharpened the estimated LMMR slope dramatically.

We conclude from this that the option expiration dates (which are known in advance) have some bearing on the evolution of the whole implied volatility surface. In other words, the periodic pattern is not merely a commentary on the LMMR fitting procedure, but contains information about the systematic behaviour of market option prices. This phenomenon is not easy to see directly from implied volatility data, but is revealed clearly once LMMR has been used as a basis to filter out stochastic volatility effects. In Section 3, we present a theory based on a periodic variation of the speed of the volatility driving process that accounts for this pattern. It is based on modifying the asymptotic theory for time-varying parameters.

2.3.1 LMMR Fit to Restricted Data

If we restrict the range of options included in the LMMR fit so that very short-dated options are mainly excluded, the stability of the fitted parameter improves considerably. We take options whose LMMR is the range

$$-2 < \text{LMMR} < 0.15.$$

This region is sketched in the top plot of Figure 5: most long-dated options are included, but very few as the time-to-maturity gets shorter. The bottom plot shows the improvement in parameter stability, as compared with Figure 3. The periodic variation in the slope is no longer seen. Note however this does not solve the problem of the separate strands for option of each maturity seen in Figure 1. In other words, the in-sample fits to the longer options is still relatively unsatisfactory. The extension we introduce in Section 3 will address both problems (stability and in-sample fit) without removing the short options as in Figure 5.

2.4 Fitting LMMR Maturity-by-Maturity

Many pricing models give rise to predicted implied volatility skews that fit the data well at fixed maturities (for example [8, 9]). This is not surprising because the implied volatility skew is quite smooth as a function of strike and any theory with reasonable properties (asymmetric return distribution, leptokurtosis) should be able to interpolate across strikes very well. The problem is going across maturities, which we try to achieve in this paper.

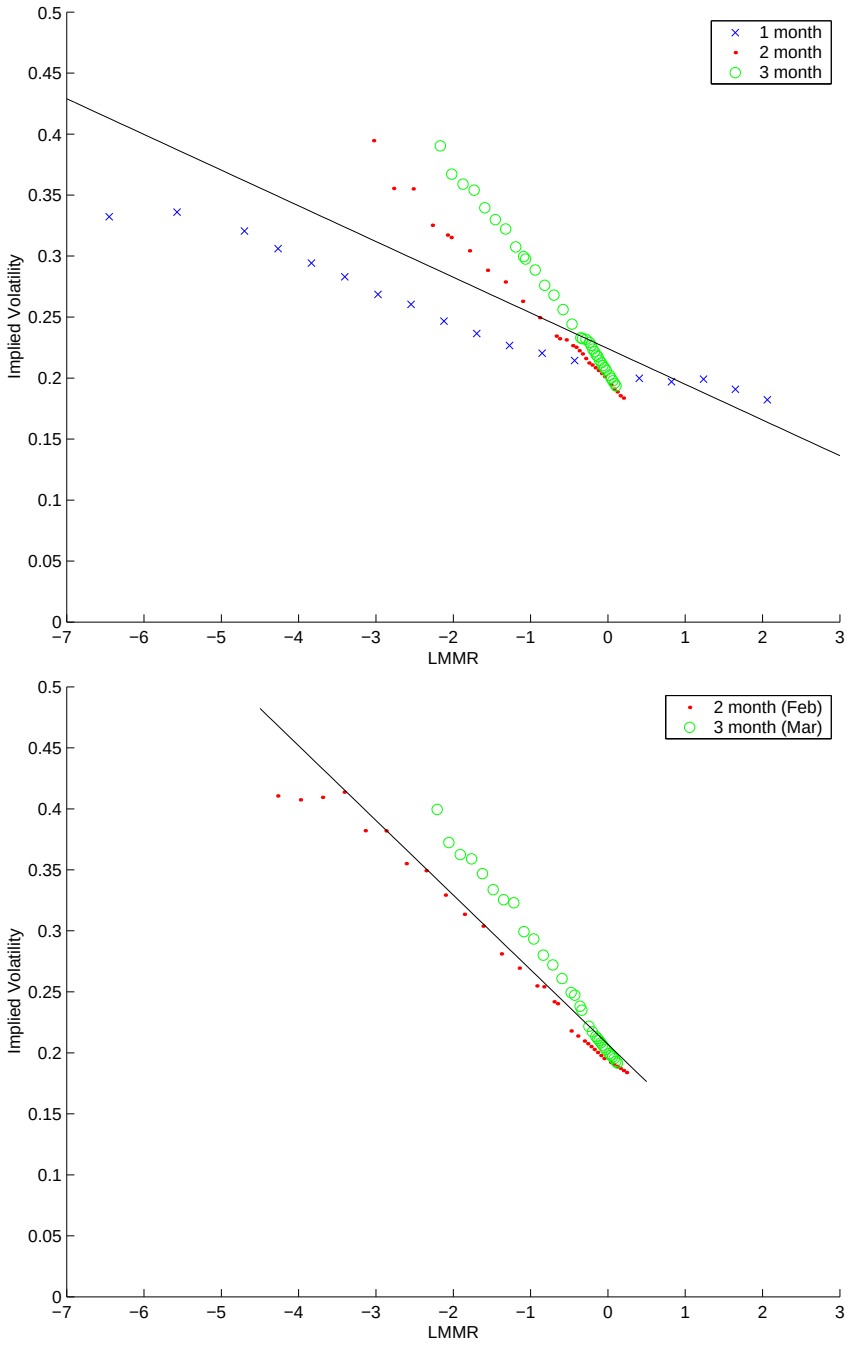

Figure 4: *In-sample LMMR fit the last day before a jump in the fitted slope (January 18, top)and after (January 19, bottom). Note that the shortest option has disappeared from data we are using in the fit.*

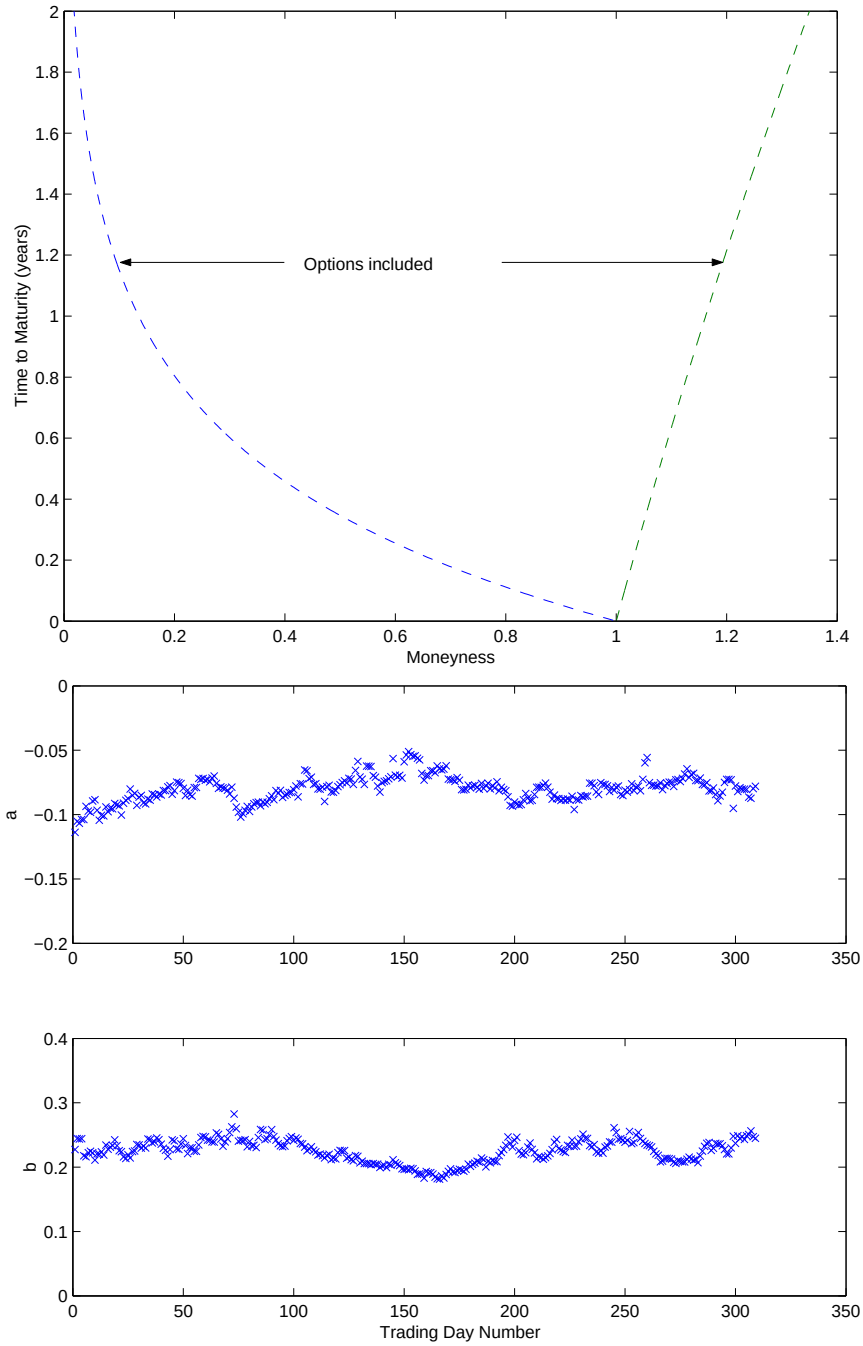

Figure 5: *Range of options included in restricted LMMR fit (top). The daily fitted LMMR parameters are shown in the bottom plot. Statistics: Mean* $(a) = -0.0801$, *Std* $(a) = 0.0100$; *Mean* $(b) = 0.2251$, *Std* $(b) = 0.0180$.

The evidence so far indicates that the slope a in (1) should depend on t and T in any modified model that will fit the data better. Many theories are in practice calibrated maturity-by-maturity. As an empirical attempt to understand the variation in a, we fit the LMMR formula each day to obtain estimates $a_{(t,T)}$ and $b_{(t,T)}$ that depend on the day t and the maturity T. In Figure 6, we plot $a_{(t,T)}$ against $T-t$ which shows that there is a systematic variation of a with $T-t$. From short-dated options, there is a sharp decay which seems to flatten as $T-t$ increases. Empirically then we might want to vary a like

$$a \sim -c(T-t)^q \qquad 0 < q < 1,\ c > 0.$$

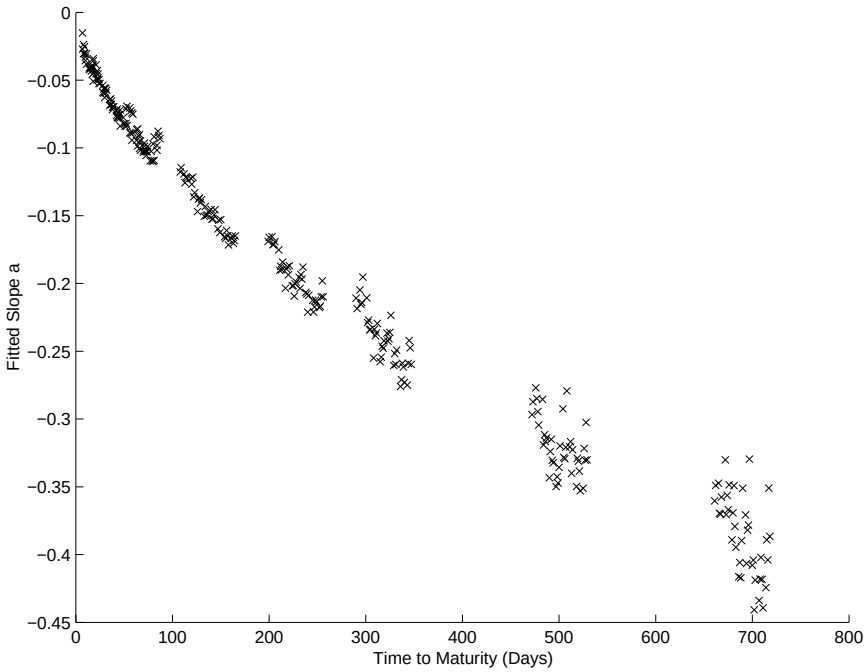

Figure 6: *LMMR slopes from fits performed daily and maturity-by-maturity as a function of time-to-expiration, using observations in January & February 2000.*

As an example, we try $q = 1/2$, which captures the square-root decay of the term-structure discussed in Section 1. We fit implied volatilities daily to the *square-root formula*:

$$I = A\frac{\log(K/S)}{\sqrt{T-t}} + B, \tag{4}$$

and estimate the slope and intercept coefficients A and B. Figure 7 shows the fit to the new square-root formula on a particular day. The separate strands for each maturity are still there, but the slopes are more closely lined up. There is an improvement in the stability of the fitted parameters as shown in Figure 8.

We conclude that we would like to modify the theory so that it

- produces good fits when using options data over a range of maturities;

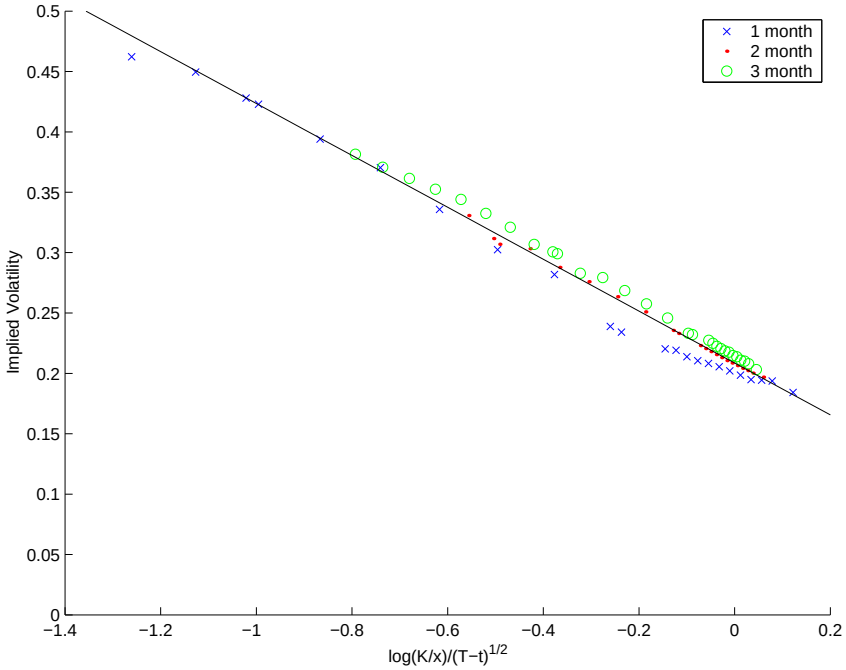

Figure 7: *Implied volatility as a function of* $\log(K/S)/\sqrt{T-t}$ *on January 12, 2000, for options with at least two and at most* 93 *days to maturity.*

- exhibits stability over time of estimated parameters;
- explains the periodic behaviour associated with expiration dates;
- is consistent with a stochastic volatility no-arbitrage derivation.

It is the last feature that prevents us from simply using the square-root formula. While it performs well empirically, it is not the product of a model (as far as we know), so having estimated A and B in (4), it is not clear what to do with them in terms of pricing other exotic derivatives or risk-management problems.

In the next section, we analyze a class of models that manage to display the properties listed above. We begin in Section 3 by establishing the asymptotic theory which takes into account time-dependent volatility parameters. The reader interested mainly in the application can skip the mathematical proofs and go directly to the implications for implied volatility approximation presented in Section 3.6.

3 Time-Dependent Parameters

We now discuss a class of mean-reverting stochastic volatility models of the underlying stock price with general (deterministic) time-dependent volatility parameters $\alpha(t), \nu(t), m(t)$ and $\rho(t)$ in (2). The main difficulty in proving the accuracy of an expansion in powers of the characteristic speed of the volatility driving process is the nondifferentiability of the option payoff at the strike. We show in Sections 3.1-3.5 how to tackle this with a regularization method, and the result is given in Theorem 1 below.

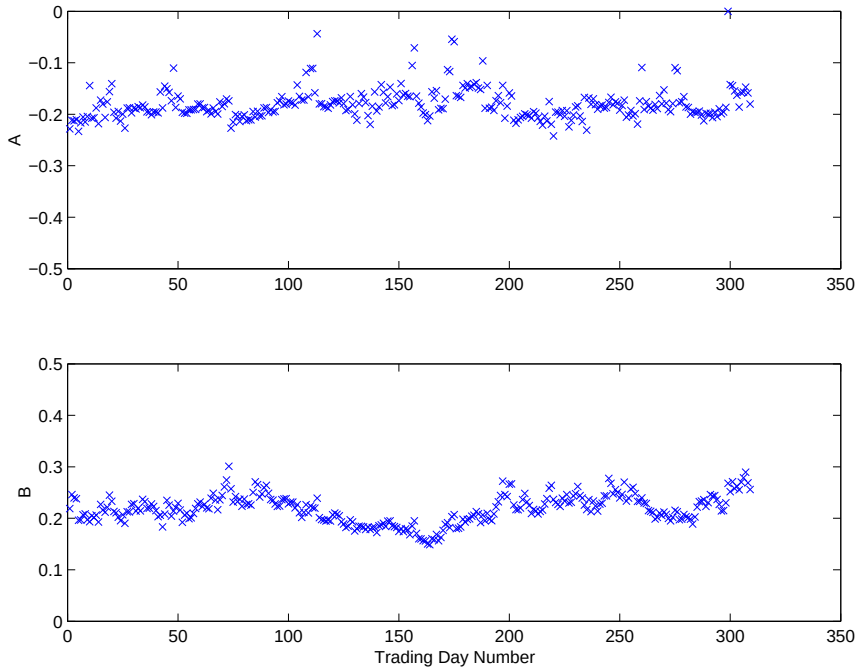

Figure 8: *Daily fitted slope A & intercepts B for options with at least* 2 *and at most* 93 *days to maturity fit to an affine function of* $\log(K/S)/\sqrt{T-t}$. *Statistics: Mean* $(A) = -0.1806$, *Std* $(A) = 0.0299$; *Mean* $(B) = 0.2177$, *Std* $(B) = 0.0272$.

In Section 3.6, we give the important application of the mathematical results for calibration from implied volatility. We discuss in Section 4 the special case where *only* α is time-dependent, which is used in the data analysis of Section 5.

3.1 Models and Derivative Pricing

We assume a probability space $(\Omega, \mathcal{F}, I\!P)$ and write the class of models we study under the real-world measure $I\!P$ as

$$\begin{aligned} dS_t^\varepsilon &= \mu S_t^\varepsilon \, dt + f(Y_t^\varepsilon) S_t^\varepsilon \, dW_t \\ dY_t^\varepsilon &= \frac{1}{\varepsilon}\alpha(t)(m(t) - Y_t^\varepsilon) \, dt + \frac{1}{\sqrt{\varepsilon}}\nu(t)\sqrt{2\alpha(t)} \, d\hat{Z}_t, \end{aligned} \tag{5}$$

where W and $\hat{Z}$ are standard Brownian motions with instantaneous correlation $\rho(t) \in (-1, 1)$:

$$I\!E\{dW_t \, d\hat{Z}_t\} = \rho(t) \, dt.$$

The volatility function f, and its reciprocal $1/f$, the local mean-reversion speed α and the function ν are assumed positive and bounded. The function m is assumed bounded.

The constant $\varepsilon > 0$ is small to represent *fast* mean-reversion. Now $\alpha(t)/\varepsilon$ is a measure of the *local* speed of the process and $\nu(t)$ a measure of the local size of volatility fluctuations and we are interested in asymptotic expansions in the limit $\varepsilon \downarrow 0$.

As is standard in the practical application of such incomplete market models, we assume that the market *selects* an equivalent martingale (pricing) measure $I\!P^\star \equiv I\!P$ under which

$(S^\varepsilon, Y^\varepsilon)$ evolves according to

$$\begin{aligned} dS_t^\varepsilon &= rS_t^\varepsilon\,dt + f(Y_t^\varepsilon)S_t^\varepsilon\,dW_t^\star \\ dY_t^\varepsilon &= \left[\frac{1}{\varepsilon}\alpha(t)(m(t)-Y_t^\varepsilon) - \frac{\nu(t)\sqrt{2\alpha(t)}}{\sqrt{\varepsilon}}\Lambda(t,Y_t^\varepsilon)\right]dt + \frac{1}{\sqrt{\varepsilon}}\nu(t)\sqrt{2\alpha(t)}\,d\hat{Z}_t^\star, \end{aligned} \tag{6}$$

where $W^\star$ and $\hat{Z}^\star$ are standard $\mathbb{P}^\star$-Brownian motions with instantaneous correlation $\rho(t) \in (-1,1)$:

$$\mathbb{E}^\star\{dW_t^\star\,d\hat{Z}_t^\star\} = \rho(t)\,dt.$$

Here, $r \geq 0$ is the riskless interest rate, assumed constant, and

$$\Lambda(t,y) = \rho(t)\frac{\mu - r}{f(y)} + \gamma(t,y)\sqrt{1-\rho(t)^2}$$

is the combined market price of volatility risk, including the volatility risk premium $\gamma(t,y)$, which characterizes the risk-neutral measure $\mathbb{P}^\star$ chosen by the market. We assume that γ is a bounded function of (t,y) only, and therefore that Y^ε is a Markov process under $\mathbb{P}^\star$.

We consider a European call option with strike price K, for which the payoff at maturity time T is

$$H(S_T^\varepsilon) = (S_T^\varepsilon - K)^+.$$

Its price at time t is given by

$$P^\varepsilon(t,S,y) = \mathbb{E}^\star\left\{e^{-r(T-t)}H(S_T^\varepsilon) \mid S_t^\varepsilon = S, Y_t^\varepsilon = y\right\}, \tag{7}$$

using the Markov property of the pair $(S^\varepsilon, Y^\varepsilon)$. We subsequently use the shorthand notation $\mathbb{E}^\star{}_{t,S,y}$ for such conditional expectations.

Under our assumptions, the function $P^\varepsilon(t,S,y)$ is the classical solution of the associated Feynman-Kac partial differential equation (PDE)

$$\begin{aligned} &\frac{\partial P^\varepsilon}{\partial t} + \frac{1}{2}f(y)^2S^2\frac{\partial^2 P^\varepsilon}{\partial S^2} + r\left(S\frac{\partial P^\varepsilon}{\partial S} - P^\varepsilon\right) \\ &+\frac{1}{\sqrt{\varepsilon}}\nu(t)\sqrt{2\alpha(t)}\left(\rho(t)f(y)S\frac{\partial^2 P^\varepsilon}{\partial S\partial y} - \Lambda(t,y)\frac{\partial P^\varepsilon}{\partial y}\right) \\ &+\frac{1}{\varepsilon}\alpha(t)\left(\nu^2(t)\frac{\partial^2 P^\varepsilon}{\partial y^2} + (m(t)-y)\frac{\partial P^\varepsilon}{\partial y}\right) = 0 \end{aligned} \tag{8}$$

in $S > 0, y \in \mathbb{R}, t < T$, with the terminal condition being the payoff at maturity, $P^\varepsilon(T,S,y) = H(S)$.

3.2 Main Theorem

The theorem of this section describes the approximation of derivative prices we obtain from an asymptotic expansion of P^ε, the solution of (8). In order to formulate it, we define

$$\langle g\rangle_t = \frac{1}{\sqrt{2\pi\nu^2(t)}}\int_{-\infty}^{\infty} g(\xi)e^{-(\xi-m(t))^2/2\nu^2(t)}d\xi,$$

the average of g with respect to the distribution $\mathcal{N}(m(t), \nu^2(t))$, and we introduce the following time-dependent deterministic quantities:

$$\bar{\sigma}^2(t) = \langle f^2 \rangle_t, \tag{9}$$

$$\overline{\bar{\sigma}^2}(t;T) = \frac{1}{T-t}\int_t^T \bar{\sigma}^2(s)\,ds, \tag{10}$$

$$V_3^\varepsilon(t) = \frac{\sqrt{\varepsilon}\,\rho(t)\nu(t)}{\sqrt{2\alpha(t)}}\langle f(\cdot)\frac{\partial \phi}{\partial y}(t,\cdot)\rangle_t \tag{11}$$

$$V_2^\varepsilon(t) = 2V_3^\varepsilon(t) - \frac{\sqrt{\varepsilon}\,\nu(t)}{\sqrt{2\alpha(t)}}\langle \Lambda(t,\cdot)\frac{\partial \phi}{\partial y}(t,\cdot)\rangle_t \tag{12}$$

$$\overline{V}_2^\varepsilon(t;T) = \frac{1}{T-t}\int_t^T V_2^\varepsilon(s)\,ds \tag{13}$$

$$\overline{V}_3^\varepsilon(t;T) = \frac{1}{T-t}\int_t^T V_3^\varepsilon(s)\,ds, \tag{14}$$

where $\phi(t,y)$ satisfies the Poisson equation

$$\mathcal{L}_0\phi(t,y) = f^2(y) - \bar{\sigma}^2(t), \tag{15}$$

and $\varepsilon^{-1}\mathcal{L}_0$ is the infinitesimal generator of the process Y^ε (5) under $I\!P$. We give $\mathcal{L}_0$ explicitly in (19). By the boundedness assumption on f, we can (and do) choose ϕ to have a bounded first derivative in y. See [6, Section 5.2.3], for example.

Our approximation is given by the sum of the following two quantities

$$P_0(t,S) = P_{BS}\left(t,S;K,T;\sqrt{\overline{\bar{\sigma}^2}(t;T)}\right), \tag{16}$$

$$\widetilde{P_1}(t,S) = -(T-t)\left[\overline{V}_2^\varepsilon(t;T)S^2\frac{\partial^2 P_0}{\partial S^2} + \overline{V}_3^\varepsilon(t;T)S^3\frac{\partial^3 P_0}{\partial S^3}\right], \tag{17}$$

where $P_{BS}(t,S;K,T;\sigma)$ is the Black-Scholes price of the European call H with the constant volatility σ, given explicitly by the Black-Scholes formula. Note that P_0 is independent of ε, and that through the coefficients $\overline{V}_2^\varepsilon$ and $\overline{V}_3^\varepsilon$, $\widetilde{P_1}$ is proportional to $\sqrt{\varepsilon}$. In the case that the volatility parameters are constant, the approximation reduces to the one detailed in [6].

Theorem 1 *Under the boundedness assumptions on the model coefficients $f, \gamma, m, \nu, \alpha$ and ρ, at any fixed time $t_0 < T$, and fixed points $S > 0, y \in \mathcal{R}$,*

$$\lim_{\varepsilon \downarrow 0} \frac{|P^\varepsilon(t_0,S,y) - (P_0(t_0,S) + \widetilde{P_1}(t_0,S))|}{\varepsilon^{1-p}} = 0,$$

for any $p > 0$.

If the payoff H was a smooth function, the proof would simply consist in writing a PDE for the approximation error and using its probabilistic representation to control it. The error expression involves S-derivatives of the Black-Scholes price $P_{BS}(t,S)$ up to order seven.

However, implied volatilities are calculated from liquid call (and put) options, for which the payoff is not differentiable at the strike, and higher derivatives of the Black-Scholes price blow up close to maturity. We present the proof in the case of the call in this section. The case of the put can be handled trivially by put-call parity.

In the nonsmooth case of the call, the proof requires a carefully-chosen regularization of the payoff. The regularization we introduce below is consistent with the Black-Scholes PDE with time-dependent volatility. The proof of the theorem is a refinement of the arguments presented in [5] to deal with time-dependent volatility parameters. For the reader's convenience, we will repeat some of the calculations in [5] and highlight the new difficulties.

3.3 Log Variable and Operator Notation

First, it is convenient to make the change of variable $x = \log S$. With a slight abuse of notation, we continue to denote the call option price by $P^\varepsilon(t,x,y)$, and we rewrite the PDE (8) with the log-stock variable as

$$\mathcal{L}^\varepsilon P^\varepsilon = 0, \qquad x, y \in I\!R, t < T, \tag{18}$$

with the terminal condition $P(T,x,y) = h(x) = H(e^x)$, where

$$\mathcal{L}^\varepsilon = \frac{1}{\varepsilon}\mathcal{L}_0 + \frac{1}{\sqrt{\varepsilon}}\mathcal{L}_1 + \mathcal{L}_2,$$

and the operators $\mathcal{L}_0, \mathcal{L}_1$ and $\mathcal{L}_2$ are defined by

$$\mathcal{L}_0 = \alpha(t)\left(\nu^2(t)\frac{\partial^2}{\partial y^2} + (m(t)-y)\frac{\partial}{\partial y}\right) \tag{19}$$

$$\mathcal{L}_1 = \nu(t)\sqrt{2\alpha(t)}\left(\rho(t)f(y)\frac{\partial^2}{\partial x \partial y} - \Lambda(t,y)\frac{\partial}{\partial y}\right) \tag{20}$$

$$\mathcal{L}_2 = \frac{\partial}{\partial t} + \frac{1}{2}f(y)^2\frac{\partial^2}{\partial x^2} + \left(r - \frac{1}{2}f(y)^2\right)\frac{\partial}{\partial x} - r\cdot. \tag{21}$$

Similarly, we denote the Black-Scholes call formula as a function of the log stock price x by $P_{BS}(t,x;K,T;\sigma)$ and our approximation to P^ε in terms of the log variable is

$$Q^\varepsilon(t,x) = P_0(t,x) + \sqrt{\varepsilon}P_1(t,x),$$

where

$$P_0(t,x) = P_{BS}\left(t,x;K,T;\sqrt{\overline{\sigma^2}(t;T)}\right), \tag{22}$$

$$\sqrt{\varepsilon}\,P_1 = -(T-t)\mathcal{A}^\varepsilon(t;T)P_0, \tag{23}$$

and

$$\mathcal{A}^\varepsilon(t;T) = \overline{V}_3^\varepsilon(t;T)\frac{\partial^3}{\partial x^3} + (\overline{V}_2^\varepsilon(t;T)^\varepsilon - 3\overline{V}_3^\varepsilon(t;T))\frac{\partial^2}{\partial x^2} + (2\overline{V}_3^\varepsilon(t;T) - \overline{V}_2^\varepsilon(t;T))\frac{\partial}{\partial x}. \tag{24}$$

3.4 Regularization

We begin by regularizing the payoff, which is a call option, by replacing it with the Black-Scholes price of a call with fixed volatility

$$\sigma_0 := \sqrt{\overline{\bar{\sigma}^2}(t_0; T)},$$

where $\overline{\bar{\sigma}^2}$ was defined in (10), and time to maturity δ. We define

$$h^{\delta,t_0}(x) := P_{BS}(T, x; K, T+\delta; \sigma_0),$$

which can also be written $h^{\delta,t_0}(x) = P_{BS}(T-\delta, x; K, T; \sigma_0)$, because the Black-Scholes formula is a function of time-to-maturity. Note that in the unregularized case, $\delta = 0$, we have $h^{0,t_0} = h$.

The Black-Scholes call pricing function P_{BS} in log variable is given explicitly by

$$\begin{aligned} P_{BS}(t, x; K, T; \sigma_0) &= e^x N(d_1) - K e^{-r(T-t)} N(d_2) \\ N(z) &= \frac{1}{\sqrt{2\pi}} \int_{-\infty}^{z} e^{-y^2/2}\, dy \\ d_1 &= \frac{x - \log K}{\sigma_0\sqrt{T-t}} + \frac{(r + \frac{1}{2}\sigma_0^2)}{\sigma_0}\sqrt{T-t} \\ d_2 &= d_1 - \sigma_0\sqrt{T-t}. \end{aligned} \tag{25}$$

For $\delta > 0$, this new payoff is smooth in x. The price $P^{\varepsilon,\delta}(t, x, y)$ of the option with the regularized payoff solves

$$\begin{aligned} \mathcal{L}^\varepsilon P^{\varepsilon,\delta} &= 0, \qquad t < T; x, y \in I\!R \\ P^{\varepsilon,\delta}(T, x, y) &= h^{\delta,t_0}(x). \end{aligned} \tag{26}$$

Let $Q^{\varepsilon,\delta}(t, x)$ denote the following approximation to the regularized option price:

$$P^{\varepsilon,\delta} \approx Q^{\varepsilon,\delta} := P_0^\delta + \sqrt{\varepsilon} P_1^\delta,$$

where $P_0^\delta(t, x)$ is the solution of

$$\langle \mathcal{L}_2 \rangle_t P_0^\delta = 0, \qquad P_0^\delta(T, x) = h^{\delta,t_0}(x), \tag{27}$$

and

$$\langle \mathcal{L}_2 \rangle_t = \frac{\partial}{\partial t} + \frac{1}{2}\bar{\sigma}^2(t)\frac{\partial^2}{\partial x^2} + \left(r - \frac{1}{2}\bar{\sigma}^2(t)\right)\frac{\partial}{\partial x} - r\cdot,$$

that is the Black-Scholes operator (in the log-stock variable) with time-dependent volatility $\bar{\sigma}^2(t) = \langle f^2 \rangle_t$, which was defined in (9). The correction term $\sqrt{\varepsilon} P_1^\delta(t, x)$ is the solution to the following PDE with a source term:

$$\langle \mathcal{L}_2 \rangle_t (\sqrt{\varepsilon} P_1^\delta) = \left(V_3^\varepsilon(t)\frac{\partial^3}{\partial x^3} + (V_2^\varepsilon(t) - 3V_3^\varepsilon(t))\frac{\partial^2}{\partial x^2} + (2V_3^\varepsilon(t) - V_2^\varepsilon(t))\frac{\partial}{\partial x} \right) P_0^\delta, \tag{28}$$

with the terminal condition $P_1^\delta(T, x) = 0$. It is given explicitly by

$$\sqrt{\varepsilon} P_1^\delta = -(T-t)\mathcal{A}^\varepsilon(t; T) P_0^\delta, \tag{29}$$

where $\mathcal{A}^\varepsilon(t; T)$ was defined in (24).

3.5 Lemmas and Proof of Theorem

We establish the following pathway to proving Theorem 1. In the following, constants may depend on (t_0, T, x, y) but not on (ε, δ):

Lemma 1 *Fix the point (t_0, x, y) where $t_0 < T$. There exist constants $\delta_1 > 0$, $\varepsilon_1 > 0$ and $c_1 > 0$ such that*

$$|P^{\varepsilon}(t_0, x, y) - P^{\varepsilon,\delta}(t_0, x, y)| \leq c_1 \delta$$

for all $0 < \delta < \delta_1$ and $0 < \varepsilon < \varepsilon_1$.

This establishes that the solutions to the regularized and unregularized problems are close.

Lemma 2 *Fix the point (t_0, x, y) where $t_0 < T$. There exist constants $\delta_2 > 0$, $\varepsilon_2 > 0$ and $c_2 > 0$ such that*

$$|Q^{\varepsilon}(t_0, x) - Q^{\varepsilon,\delta}(t_0, x)| \leq c_2 \delta$$

for all $0 < \delta < \delta_2$ and $0 < \varepsilon < \varepsilon_2$.

This establishes that the approximations to the regularized and unregularized prices are close.

Lemma 3 *Fix the point (t_0, x, y) where $t_0 < T$. There exist constants $\delta_3 > 0$, $\varepsilon_3 > 0$ and $c_3 > 0$ such that*

$$|P^{\varepsilon,\delta}(t_0, x, y) - Q^{\varepsilon,\delta}(t_0, x)| \leq c_3 \left(\varepsilon |\log \delta| + \varepsilon \sqrt{\frac{\varepsilon}{\delta}} + \varepsilon \right),$$

for all $0 < \delta < \delta_3$ and $0 < \varepsilon < \varepsilon_3$.

This establishes that for fixed $\delta > 0$, when the payoff is smooth, the approximation is $\mathcal{O}(\varepsilon)$.

We now show that Theorem 1 follows from these lemmas.

Proof of Theorem 1. Take $\bar{\delta} = \min(\delta_1, \delta_2, \delta_3)$ and $\bar{\varepsilon} = \min(\varepsilon_1, \varepsilon_2, \varepsilon_3)$. Then, using lemmas 1, 2 and 3, we obtain

$$\begin{aligned} |P^{\varepsilon} - Q^{\varepsilon}| &\leq |P^{\varepsilon} - P^{\varepsilon,\delta}| + |Q^{\varepsilon,\delta} - Q^{\varepsilon}| + |P^{\varepsilon,\delta} - Q^{\varepsilon,\delta}| \\ &\leq 2 \max(c_1, c_2) \delta + c_3 \left(\varepsilon |\log \delta| + \varepsilon \sqrt{\frac{\varepsilon}{\delta}} + \varepsilon \right), \end{aligned}$$

for $0 < \delta < \bar{\delta}$ and $0 < \varepsilon < \bar{\varepsilon}$, where the functions are evaluated at the fixed (t_0, x, y). Taking $\delta = \varepsilon$, we have

$$|P^{\varepsilon} - Q^{\varepsilon}| \leq c_4 (\varepsilon + \varepsilon |\log \varepsilon|),$$

for some fixed $c_4 > 0$, and Theorem 1 follows.

We begin by proving Lemma 3 which explains the choices of P_0, P_1 and their δ-counterparts.

3.5.1 Proof of Lemma 3

We first introduce some additional notation. Define the error $Z^{\varepsilon,\delta}$ in the approximation for the regularized problem by

$$P^{\varepsilon,\delta} = P_0^\delta + \sqrt{\varepsilon} P_1^\delta + \varepsilon Q_2^\delta + \varepsilon^{3/2} Q_3^\delta - Z^{\varepsilon,\delta},$$

for Q_2^δ and Q_3^δ stated below in (33) and (34). We can write

$$\begin{aligned}
\mathcal{L}^\varepsilon Z^{\varepsilon,\delta} &= \mathcal{L}^\varepsilon \left(P_0^\delta + \sqrt{\varepsilon} P_1^\delta + \varepsilon Q_2^\delta + \varepsilon^{3/2} Q_3^\delta - P^{\varepsilon,\delta} \right) && (30)\\
&= \frac{1}{\varepsilon} \mathcal{L}_0 P_0^\delta + \frac{1}{\sqrt{\varepsilon}} (\mathcal{L}_0 P_1^\delta + \mathcal{L}_1 P_0^\delta) && (31)\\
&\quad + (\mathcal{L}_0 Q_2^\delta + \mathcal{L}_1 P_1^\delta + \mathcal{L}_2 P_0^\delta) + \sqrt{\varepsilon} \left(\mathcal{L}_0 Q_3^\delta + \mathcal{L}_1 Q_2^\delta + \mathcal{L}_2 P_1^\delta \right)\\
&\quad + \varepsilon \left(\mathcal{L}_1 Q_3^\delta + \mathcal{L}_2 Q_2^\delta + \sqrt{\varepsilon} \mathcal{L}_2 Q_3^\delta \right)\\
&= \varepsilon \left(\mathcal{L}_1 Q_3^\delta + \mathcal{L}_2 Q_2^\delta \right) + \varepsilon^{3/2} \mathcal{L}_2 Q_3^\delta =: G^{\varepsilon,\delta} && (32)
\end{aligned}$$

because

- $P^{\varepsilon,\delta}$ solves the original equation (26): $\mathcal{L}^\varepsilon P^{\varepsilon,\delta} = 0$.
- P_0^δ and P_1^δ do not depend on y, whilst $\mathcal{L}_0$ and $\mathcal{L}_1$ defined in (19) and (20) respectively, take y-derivatives. Consequently the first two terms in (31) are zero.
- $P_0^\delta(t,x)$ is defined as the solution of (27). Therefore, the Poisson equation

  $$\mathcal{L}_0 Q_2^\delta = -\mathcal{L}_2 P_0^\delta,$$

  for Q_2^δ has a source term in the null complement of the adjoint of $\mathcal{L}_0$, and admits the solution

  $$Q_2^\delta(t,x,y) = -\frac{1}{2}\phi(t,y) \left(\frac{\partial^2 P_0^\delta}{\partial x^2} - \frac{\partial P_0^\delta}{\partial x} \right), \tag{33}$$

  where ϕ satisfies (15) and has bounded first derivative in y. Consequently, with this choice of Q_2^δ, the third term in (31) is zero.
- Similarly, we choose Q_3^δ to be a solution of the Poisson equation

  $$\mathcal{L}_0 Q_3^\delta = -(\mathcal{L}_1 Q_2^\delta + \mathcal{L}_2 P_1^\delta), \tag{34}$$

  where the solvability condition is ensured by our choice of P_1^δ given in (29), and so the fourth term in (31) is zero.

At the terminal time T, we have

$$Z^{\varepsilon,\delta}(T,x,y) = \varepsilon \left(Q_2^\delta(T,x,y) + \sqrt{\varepsilon} Q_3^\delta(T,x,y) \right) =: H^{\varepsilon,\delta}(x,y), \tag{35}$$

where we have used the terminal conditions $P^{\varepsilon,\delta}(T,x,y) = P_0^\delta(T,x) = h^{\delta,t_0}(x)$ and $P_1^\delta(T,x) = 0$. This assumes smooth derivatives of P_0^δ at $t = T$ which is the case because h^{δ,t_0} is smooth.

The explicit expressions for $G^{\varepsilon,\delta}$ and $H^{\varepsilon,\delta}$ involve derivatives in x of P_0^δ up to order seven, as can be seen from substituting from (33) and (34) into (32) and (35). The algebra is given in [5, Appendix A]. Because of the smoothness of $G^{\varepsilon,\delta}$ and $H^{\varepsilon,\delta}$, and the regularity of the coefficients of the diffusion $(X^\varepsilon, Y^\varepsilon)$, we have the probabilistic representation of the solution of equation (30), $\mathcal{L}^\varepsilon Z^{\varepsilon,\delta} = G^{\varepsilon,\delta}$ with terminal condition $H^{\varepsilon,\delta}$:

$$Z^{\varepsilon,\delta}(t,x,y) = I\!E^\star{}_{t,x,y}\left\{e^{-r(T-t)}H^{\varepsilon,\delta}(X_T^\varepsilon, Y_T^\varepsilon) - \int_t^T e^{-r(s-t)}G^{\varepsilon,\delta}(s, X_s^\varepsilon, Y_s^\varepsilon)ds\right\}.$$

The following estimates (36) and (37) can be obtained by a slight adaptation of the proof of Lemma 3 in [5]. They rely on standard results about the growth of solutions of Poisson equations like (15), as given in [6, Section 5.2.2] for example, and explicit calculation of derivatives in x of up to order seven of the Black-Scholes formula. The main modification in the argument that allows us to exploit the Black-Scholes formula is to note that we can write $P_0^\delta(t,x)$, defined by (27), in terms of P_{BS}, but with a volatility parameter $\tilde{\sigma}(t;T)$, where

$$\tilde{\sigma}^2(t;T) := \frac{1}{T+\delta-t}\left(\int_t^T \bar{\sigma}^2(s)\,ds + \delta\sigma_0\right),$$

that depends on t and δ. Note, however, that $\tilde{\sigma}$ is uniformly bounded because of the bound on f.

There exists a constant $c > 0$ such that

$$\begin{aligned} |I\!E^\star{}_{t,x,y}\left\{\int_t^T e^{-r(s-t)}G^{\varepsilon,\delta}(X_s^\varepsilon, Y_s^\varepsilon)ds\right\}| &\leq c\left\{\varepsilon + \varepsilon|\log(\delta)| + \varepsilon\sqrt{\varepsilon/\delta}\right\} \qquad (36)\\ |I\!E^\star{}_{t,x,y}\left\{H^{\varepsilon,\delta}(X_T^\varepsilon, Y_T^\varepsilon)\right\}| &\leq c\left\{\varepsilon + \varepsilon\sqrt{\varepsilon/\delta}\right\}, \qquad (37)\end{aligned}$$

and therefore also for (t_0,x,y) fixed with $t_0 < T$,

$$\begin{aligned} |P^{\varepsilon,\delta} - Q^{\varepsilon,\delta}| &= |\varepsilon Q_2^\delta + \varepsilon^{3/2}Q_3^\delta - Z^{\varepsilon,\delta}| \\ &\leq c_3\left\{\varepsilon + \varepsilon|\log(\delta)| + \varepsilon\sqrt{\varepsilon/\delta}\right\}, \qquad (38)\end{aligned}$$

for some $c_3 > 0$, since Q_2^δ and Q_3^δ evaluated at $t_0 < T$ can be expressed in terms of derivatives of P_{BS} with respect to x, and so can be uniformly bounded, as shown explicitly in [5].

3.5.2 Proof of Lemma 1

We begin with the probabilistic representation of $P^{\varepsilon,\delta}$

$$P^{\varepsilon,\delta}(t_0,x,y) = I\!E^\star{}_{t_0,x,y}\left\{e^{-r(T-t_0)}h^{\delta,t_0}(X_T^\varepsilon)\right\},$$

and define a new process $(\tilde{X}_t^\varepsilon)$ by

$$d\tilde{X}_t^\varepsilon = \left(r - \frac{1}{2}\tilde{f}(t,Y_t^\varepsilon)^2\right)dt + \tilde{f}(t,Y_t^\varepsilon)\left(\sqrt{1-\rho^2}\,d\hat{W}_t^\star + \rho\,d\hat{Z}_t^\star\right),$$

where $(\hat{W}_t^\star)$ is a Brownian motion independent of $(\hat{Z}_t^\star)$, (Y_t^ε) is still a solution of (6) and

$$\tilde{f}(t,y) = \begin{cases} f(y) & \text{for } t \le T \\ \sigma_0 & \text{for } t > T. \end{cases}$$

Then we can write

$$P^{\varepsilon,\delta}(t_0,x,y) = I\!E^\star{}_{t_0,x,y}\left\{e^{-r(T-t_0+\delta)}h(\tilde{X}^\varepsilon_{T+\delta})\right\},$$

because of the choice of regularized payoff h^{δ,t_0}. We recall that

$$P^{\varepsilon}(t_0,x,y) = I\!E^\star{}_{t_0,x,y}\left\{e^{-r(T-t_0)}h(\tilde{X}^\varepsilon_{T})\right\},$$

and we use the iterated expectations formula

$$\begin{aligned} & P^{\varepsilon,\delta}(t_0,x,y) - P^{\varepsilon}(t_0,x,y) \\ = \;& I\!E^\star{}_{t_0,x,y}\left\{I\!E^\star{}_{t_0,x,y}\left\{e^{-r(T-t_0+\delta)}h(\tilde{X}^\varepsilon_{T+\delta}) - e^{-r(T-t_0)}h(\tilde{X}^\varepsilon_{T}) \mid (\hat{Z}^\star_s)_{t_0\le s\le T}\right\}\right\} \end{aligned}$$

to obtain a representation of this price difference in terms of the Black-Scholes function P_{BS} which is smooth away from the terminal date T. In the uncorrelated case this representation corresponds to the Hull-White formula [7]. In the correlated case, as considered here, this formula is in [10], and can be found in [6](2.8.3).

It is simple to compute explicitly the conditional distribution of $\tilde{X}^\varepsilon_T$ given the path of the second Brownian motion $(\hat{Z}^\star_s)_{t_0\le s\le T}$. One obtains

$$\mathcal{D}(\tilde{X}^\varepsilon_T | (\hat{Z}^\star_s)_{t_0\le s\le T}, \tilde{X}^\varepsilon_{t_0} = x, Y^\varepsilon_{t_0} = y) = \mathcal{N}(m_1^\varepsilon, v_1^\varepsilon),$$

where the mean and variance are given by

$$\begin{aligned} m_1^\varepsilon &= x + \xi_{t_0,T} + \left(r - \frac{1}{2}\overline{\sigma_\rho^2}\right)(T-t_0) \\ v_1^\varepsilon &= \overline{\sigma_\rho^2}(T-t_0), \end{aligned}$$

using the definitions

$$\begin{aligned} \xi_{t_0,T} &= \rho\int_{t_0}^T \tilde{f}(s,Y_s^\varepsilon)\,d\hat{Z}_s^\star - \frac{1}{2}\rho^2\int_{t_0}^T \tilde{f}(s,Y_s^\varepsilon)^2 ds \qquad (39) \\ \overline{\sigma_\rho^2} &= \frac{1-\rho^2}{T-t_0}\int_{t_0}^T \tilde{f}(s,Y_s^\varepsilon)^2 ds. \end{aligned}$$

It follows from the calculation that leads to the Black-Scholes formula that

$$I\!E^\star{}_{t_0,x,y}\{e^{-r(T-t_0)}h(\tilde{X}^\varepsilon_T) \mid (\hat{Z}^\star_s)_{t_0\le s\le T}\} = P_{BS}\left(t_0, x+\xi_{t_0,T}; K, T; \sqrt{\overline{\sigma_\rho^2}}\right).$$

Similarly, we compute

$$\mathcal{D}(\tilde{X}^\varepsilon_{T+\delta} \mid (\hat{Z}^\star_s)_{t\le s\le T}, \tilde{X}^\varepsilon_{t_0} = x, Y^\varepsilon_{t_0} = y) = \mathcal{N}(m_2^\varepsilon, v_2^\varepsilon),$$

where the mean and variance are given by

$$\begin{aligned} m_2^\varepsilon &= x + \xi_{t_0,T} + r\delta + \left(r - \frac{1}{2}\overline{\sigma^2_{\rho,\delta}}\right)(T-t_0) \\ v_2^\varepsilon &= \overline{\sigma^2_{\rho,\delta}}(T-t_0), \end{aligned}$$

and we define

$$\overline{\sigma^2_{\rho,\delta}} = \overline{\sigma^2_\rho} + \frac{\delta\sigma_0^2}{T-t_0}.$$

Therefore,

$$I\!E^\star_{t_0,x,y}\{e^{-r(T-t_0+\delta)}h(\tilde{X}^\varepsilon_{T+\delta}) \mid (\hat{Z}^\star_s)_{t_0\le s\le T}\} = e^{-r\delta}P_{BS}\left(t_0, x+\xi_{t_0,T}+r\delta; K, T; \sqrt{\overline{\sigma^2_{\rho,\delta}}}\right),$$

and we can write

$$\begin{aligned} & P^{\varepsilon,\delta}(t_0,x,y) - P^\varepsilon(t_0,x,y) \\ = \; & I\!E^\star_{t_0,x,y}\left\{e^{-r\delta}P_{BS}\left(t_0, x+\xi_{t_0,T}+r\delta; K, T; \sqrt{\overline{\sigma^2_{\rho,\delta}}}\right) - P_{BS}\left(t_0, x+\xi_{t_0,T}; K, T; \sqrt{\overline{\sigma^2_\rho}}\right)\right\}. \end{aligned}$$

Using the explicit representation (25) and that $\sqrt{\overline{\sigma^2_\rho}}$ is bounded above and below, since $f(y)$ is, we find

$$\begin{aligned} \left| e^{-r\delta}P_{BS}\left(t_0, x+\xi_{t_0,T}+r\delta; K, T; \sqrt{\overline{\sigma^2_{\rho,\delta}}}\right) \right. & - \left. P_{BS}\left(t_0, x+\xi_{t_0,T}; K, T; \sqrt{\overline{\sigma^2_\rho}}\right)\right| \\ & \le \delta c(e^{\xi_{t_0,T}}[|\xi_{t_0,T}|+1]+1) \end{aligned}$$

for some c and for δ small enough. Using the definition (39) of $\xi_{t_0,T}$ and the existence of its exponential moments, we thus find that

$$|P^\varepsilon(t_0,x,y) - P^{\varepsilon,\delta}(t_0,x,y)| \le c_1\delta$$

for some c_1 and for δ small enough.

3.5.3 Proof of Lemma 2

From the definition (23) of the correction $\sqrt{\varepsilon}P_1$ and the corresponding definition (29) of the correction $\sqrt{\varepsilon}P_1^\delta$, we deduce

$$Q^{\varepsilon,\delta} - Q^\varepsilon = (1-(T-t)\mathcal{A}^\varepsilon(t;T))\,(P_0^\delta - P_0).$$

From the definitions (13) and (14) of the V_i's and the boundedness of the derivative of the solution of the Poisson equation (15), it follows that

$$\max(|\overline{V_3}^\varepsilon|, |\overline{V_2}^\varepsilon|) \le c\sqrt{\varepsilon}$$

for some constant $c > 0$.

We can write

$$P_0^\delta(t_0, x) = P_{BS}(t_0 - \delta, x; K, T, \sigma_0), \tag{40}$$

because P_0^δ satisfies the Black-Scholes PDE with time-varying (deterministic) volatility (27), whose solution at time t_0 is well-known to be given simply by the Black-Scholes formula evaluated with the root-mean-square volatility over the path from t_0 to $T + \delta$. In this case, the appropriate mean-square volatility, using the definition of the regularized payoff h^{δ,t_0}, is given by

$$\frac{1}{T + \delta - t_0}\left(\int_{t_0}^{T} \bar{\sigma}^2(s)\, ds + \delta\sigma_0^2\right) = \frac{1}{T + \delta - t_0}\left((T - t_0)\sigma_0^2 + \delta\sigma_0^2\right) = \sigma_0^2,$$

where we used the definition $\sigma_0^2 = \overline{\bar{\sigma}^2}(t_0; T)$. Note that (40) holds only at time t_0.

We also have

$$P_0(t_0, x) = P_{BS}(t_0, x; K, T; \sigma_0). \tag{41}$$

Using the explicit formula (25), it is easily seen that P_{BS} and its successive derivatives with respect to x are differentiable in t at any $t < T$. Therefore, from (40) and (41), we conclude that for (t_0, x, y) fixed with $t_0 < T$:

$$|Q^\varepsilon(t_0, x) - Q^{\varepsilon,\delta}(t_0, x)| \le c_2\delta$$

for some $c_2 > 0$ and δ small enough.

3.6 Implications for Implied Volatility Approximation

To summarize, the asymptotic approximation at a generic time $t < T$ for the call option price P^ε (in the original stock variable S), defined in (7), is given by

$$P^\varepsilon(t, S, y) = P_{BS} - (T - t)\left[\overline{V}_2^\varepsilon(t; T)S^2\frac{\partial^2 P_{BS}}{\partial S^2} + \overline{V}_3^\varepsilon(t; T)S^3\frac{\partial^3 P_{BS}}{\partial S^3}\right] + \mathcal{O}(\varepsilon^p),$$

for any $p < 1$, where the argument of the Black-Scholes formula P_{BS} is $\left(t, S; K, T; \sqrt{\overline{\bar{\sigma}^2}(t; T)}\right)$, $\overline{\bar{\sigma}^2}$ is defined in (10) and $\overline{V}_2^\varepsilon(t; T)$ and $\overline{V}_3^\varepsilon(t; T)$ in (13) and (14) respectively. This is analogous to the constant parameter case given in [6] with the replacements

$$\begin{aligned} \bar{\sigma}^2 &\mapsto \overline{\bar{\sigma}^2}(t; T) \\ V_2 &\mapsto \overline{V}_2^\varepsilon(t; T) \\ V_3 &\mapsto \overline{V}_3^\varepsilon(t; T). \end{aligned}$$

The corresponding approximation for the implied volatility, can be obtained from its defining relationship

$$P_{BS}(t, S; K, T; I) = P^\varepsilon(t, S, y).$$

Formally inserting an expansion for implied volatility

$$I = I_0 + \sqrt{\varepsilon}I_1 + \varepsilon I_2 + \cdots,$$

a simple calculation, given for example in [6, Section 5.3], yields

$$\begin{aligned} I_0 &= \sqrt{\overline{\bar{\sigma}^2}(t;T)}, \\ \sqrt{\varepsilon} I_1 &= -(T-t)\frac{\left[\overline{V}^{\varepsilon}_2(t;T) S^2 \frac{\partial^2 P_{BS}}{\partial S^2} + \overline{V}^{\varepsilon}_3(t;T) S^3 \frac{\partial^3 P_{BS}}{\partial S^3}\right]}{\frac{\partial P_{BS}}{\partial \sigma}}. \end{aligned}$$

Using the explicit expressions, we obtain the approximation

$$I \approx a(t;T)\frac{\log(K/S)}{T-t} + b(t;T), \tag{42}$$

where

$$\begin{aligned} a(t;T) &= -\frac{1}{(\overline{\bar{\sigma}^2}(t;T))^{3/2}} \overline{V}^{\varepsilon}_3(t;T) \\ b(t;T) &= \sqrt{\overline{\bar{\sigma}^2}(t;T)} - a(t;T)\left(r + \frac{3}{2}\overline{\bar{\sigma}^2}(t;T)\right) - \frac{\overline{V}^{\varepsilon}_2(t;T)}{\sqrt{\overline{\bar{\sigma}^2}(t;T)}}, \end{aligned} \tag{43}$$

and we do not denote the ε dependence of a and b.

Finally, we note that there is an extension to the asymptotic approximations for exotic options (for example American puts, barriers and Asians), similar to those presented in [6], to incorporate time-dependent volatility parameters. In this case, the approximations depend on $V_2^{\varepsilon}(t)$ and $V_3^{\varepsilon}(t)$.

4 Calibration

Typically, time-dependent parameters are calibrated by first interpolating the observed term-structure of implied volatilities and then differentiating with respect to maturity. This is not the path we follow. Instead we will take advantage of the systematic and near-periodic time-variation of a quantity derived from S&P 500 implied volatilities, as seen in Figure 3.

We will show that taking the speed $\alpha(t)$ of the volatility driving process to be periodically time-varying, with the typical size of the fluctuations ν, the mean-level m and the correlation ρ constant, is sufficient to capture the periodicity in the fitted skew parameter observed in Figure 3. In this case, the averaging $\langle\cdot\rangle$ does *not* depend on t, but we still have time-dependent $V_2^{\varepsilon}(t), V_3^{\varepsilon}(t), a(t;T), b(t;T)$. Furthermore, $\overline{\bar{\sigma}^2}(t;T) = \bar{\sigma}^2$ is constant and can be estimated from long-run historical returns as usual.

Since now only α is time-dependent, it follows from (13), (14) and (43) that

$$\begin{aligned} a(t;T) &= \frac{k_a}{T-t}\int_t^T \frac{1}{\sqrt{\alpha(s)}}\, ds \\ b(t;T) &= \bar{\sigma} + \frac{k_b}{T-t}\int_t^T \frac{1}{\sqrt{\alpha(s)}}\, ds, \end{aligned} \tag{44}$$

for some small constants k_a and k_b (of order $\sqrt{\varepsilon}$). (We remark that an alternative way to obtain a similar calibration procedure is to assume only the correlation ρ to be time-dependent, but as this seems less economically plausible, we do not pursue it here).

4.1 Calendar Function

It remains to choose a model for the time-dependence. Based on our previous analysis of the data in Section 2, we propose the following form:

$$\frac{1}{\sqrt{\alpha(t)}} = c\,(T_{n(t)} - t)^{1/2}, \tag{45}$$

for some constant c. Here $\{T_k\}$ are the option maturity dates (the third Friday of each month), and

$$n(t) = \inf\{n : T_n \geq t\},$$

the next expiration after time t. In other words, $\alpha(t)$ is a near-periodic function described by the time till the next maturity date. Clearly, there are many ways to generalize this idea, the simplest being to vary the power in (45). We will show in Section 4.2 that this choice captures well the maturity-dependent behaviour of the implied volatilities that we observed in Section 2.

Note that $\alpha(t)$ as chosen in (45) is unbounded. For convenience, we perform the calculations below with this α, but a large cutoff can be included to be consistent with the boundedness assumption made in Section 3, with a negligible effect on the results.

For simplicity, we assume the expiration dates are evenly spaced:

$$T_{k+1} - T_k =: \Delta T,$$

where in applications ΔT will be a month. From (44), we have that

$$a(t,T) = \frac{k_a}{T-t}\int_t^T (T_{n(s)} - s)^{1/2} ds.$$

Given a time t and an option expiration date T, if we decompose the time-to-maturity as

$$T - t = \Delta T(m_0 + \eta)$$

with $0 \leq \eta < 1$, we have

$$\begin{aligned}\frac{1}{T-t}\int_t^T (T_{n(s)} - s)^{1/2} ds &= \frac{1}{T-t}\left(\int_{(1-\eta)\Delta T}^{\Delta T} (\Delta T - s)^{1/2} ds + m_0 \int_0^{\Delta T} (\Delta T - s)^{1/2} ds\right) \\ &= \frac{2(\Delta T)^{1/2}}{3}\frac{m_0 + \eta^{3/2}}{m_0 + \eta}.\end{aligned}$$

Using (42), we get the following approximation for the implied volatility

$$I = A\frac{\log(K/S)}{\mathcal{T}(t,T)} + B\frac{(T-t)}{\mathcal{T}(t,T)} + \bar{\sigma}, \tag{46}$$

where we define the **effective time to maturity (ETM)** as

$$\mathcal{T}(t,T) = \frac{(T-t)}{\left(\frac{m_0+\eta^{3/2}}{m_0+\eta}\right)}. \tag{47}$$

Empirically, we show below that this choice of time variation performs well, but of course other choices may fit the data even better; we have not investigated this here.

4.2 Effective Time-to-Maturity

We plot $\mathcal{T}(t,T)$ for the model described above in Figure 9. Note that the effective time

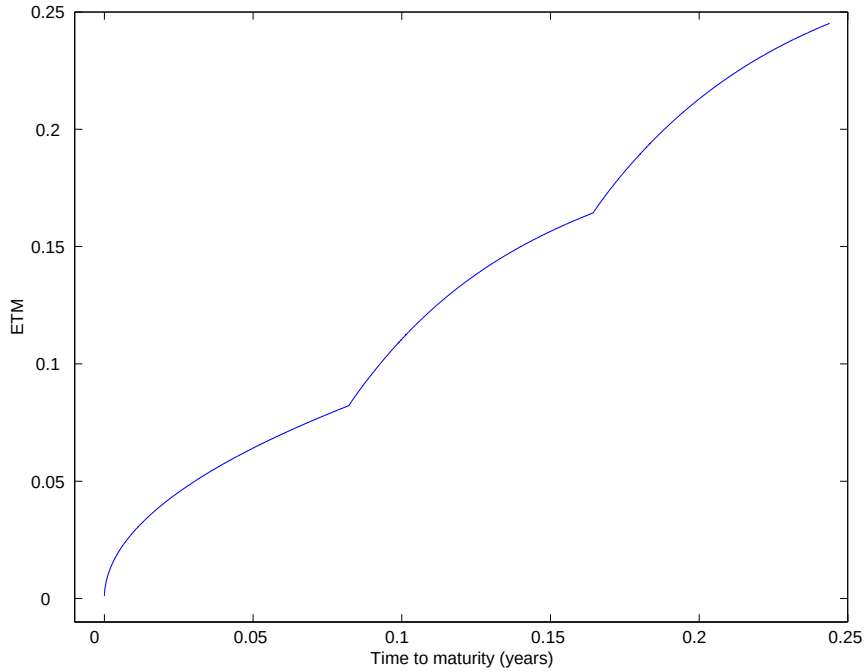

Figure 9: *Effective time to maturity (ETM) as a function of time-to-maturity for a three month option.*

runs faster close to the monthly maturity dates. Moreover, observe that if $T-t < \Delta T$ then $m_0 = 0$ and $\eta = (T-t)/(\Delta T)$ so that

$$\mathcal{T}(t,T) \sim \sqrt{T-t},$$

whereas if $T - t >> \Delta T$ then $\eta << m_0$, and therefore

$$\mathcal{T}(t,T) \sim (T-t).$$

This gives for the implied volatility

$$\begin{aligned} I &\approx A\frac{\log(K/x)}{\sqrt{T-t}} + B\sqrt{T-t} + \bar{\sigma} \qquad \text{for short maturities} \\ I &\approx A\frac{\log(K/x)}{(T-t)} + B + \bar{\sigma} \qquad \text{for long maturities.} \end{aligned}$$

Thus, for long dated options the implied volatility is approximately affine in LMMR as in (1). For short dated options the implied volatility is approximately affine in $\log(K/x)/\sqrt{T-t}$ as suggested by the observation (3) referred to in Section 1.

The kinks in Figure 9 correspond to different maturity dates T_k, and the interval in between these are here taken to be 30 days. Note that the effect of the maturity-date-dependent rate of mean reversion averages out and become negligible when the option is several maturity intervals from the actual maturity-date. However, in the last maturity period (when the option is close to maturity), it becomes a very pronounced effect.

5 Data Revisited using Time-Dependent Theory

The modified theory derived in the last section suggests to fit the implied volatility surface to a function that is affine in the two composite variables

$$\frac{\log(K/x)}{\mathcal{T}(t,T)}; \qquad \frac{(T-t)}{\mathcal{T}(t,T)}.$$

Further, the regression constant should be close to $\bar{\sigma}$ which we estimate from historical S&P 500 returns in 2000 as $\bar{\sigma} = 0.17$.

This is a multiple linear regression, but there are far more points in the direction of the first variable than the second because there are typically dozens of liquid strikes, but only three different maturities (in the data we are restricting ourselves to). Therefore in our estimation procedure we do not place the same emphasis on both variables: we first estimate B maturity-by-maturity on each day by regressing $I - \bar{\sigma}$ on $\log(K/x)/\mathcal{T}(t,T)$ to obtain estimates $B_{(t,T)}$. Since these are analogous to the intercept parameter b in the LMMR fit, they are quite stable (as were the b's in Figure 3) because they describe the basic level of the surface. Our estimate of B is fixed as the average of these estimates $B = 0.0447$.

This is approximately the average extra level of at-the-money implied volatilities over the historical volatility $\bar{\sigma}$.

Then we fit the *maturity adjusted implied volatility*

$$I - B\frac{(T-t)}{\mathcal{T}(t,T)}$$

as an affine function of $\log(K/x)/\mathcal{T}(t,T)$ by least-squares to estimate A. The residual (which includes the error in the fit and the constant $\bar{\sigma}$ is denoted R).

Figure 10 shows the improvement in the goodness-of-fit and how the effective time-to-maturity has squeezed the previously diverging strands in Figure 1 together. Next we look at the days before and after the shortest dated options disappear in a particular month. As Figure 11 and shows, there is no longer a dramatic jump in the estimated slope A.

Finally, Figure 12 shows the daily estimated slope A and the residual R. Clearly there is an improvement in stability over Figure 3 because the effect of the expiration dates has been taken into account.

As mentioned in the introduction similar goodness-of-fit and stability results were obtained with the 1993 S&P 500 dataset constructed in [1].

6 Conclusions

In this article, we have derived and tested a calibration procedure for implied volatility surfaces based on a class of stochastic volatility models. It is able to fit the S&P 500 data well across a few maturities at once (Figure 10), and also results in parameter estimates that are stable over time (Figure 12).

The asymptotic analysis of stochastic volatility models with constant parameters leads to the LMMR calibration procedure. When used to analyze S&P 500 implied volatilities,

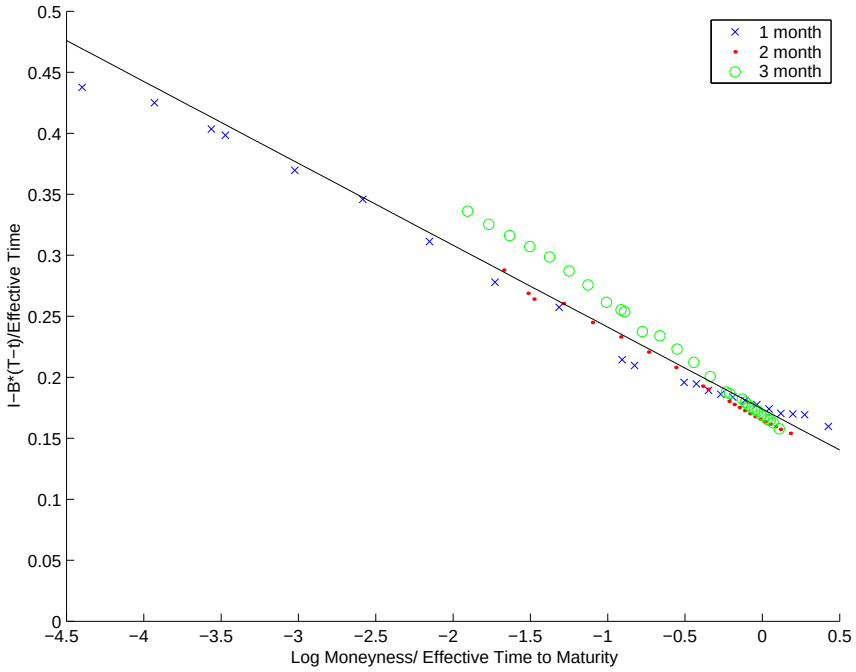

Figure 10: *Maturity-adjusted implied volatility as a function of log-moneyness to ETM on January 12, 2000, for options with at least two and at most* 93 *days to maturity. Notice the strand for the shortest maturity has been squeezed closer to the strand for the next maturity. Compare Figure 1.*

it identifies a significant near-periodic trend, closely associated with the option expiration dates the third Friday of each month.

This observation leads us to modify the class of volatility models to incorporate a time-dependent *periodic* rate of mean-reversion, which is a function of the time to the next expiration date. The asymptotic analysis produces the improved calibration method based on the effective time-to-maturity.

We do not speculate here on a market mechanism that might produce a periodic characteristic speed of mean-reversion in the volatility driving process. A behavioural model in which market makers react to impending "witching dates" and increased market volatility associated with them is a topic of future investigation.

Longer Maturities and Slow Volatility Factor

Finally we comment on the situation with options of longer maturity. In this work, we restricted our study to options of at most three months to maturity. However longer options also trade quite actively in the S&P 500 and other markets. The time-dependent theory introduced here is not designed to help with these options. As shown in Figure 13, these are not captured well by the one-factor stochastic volatility asymptotic theory.

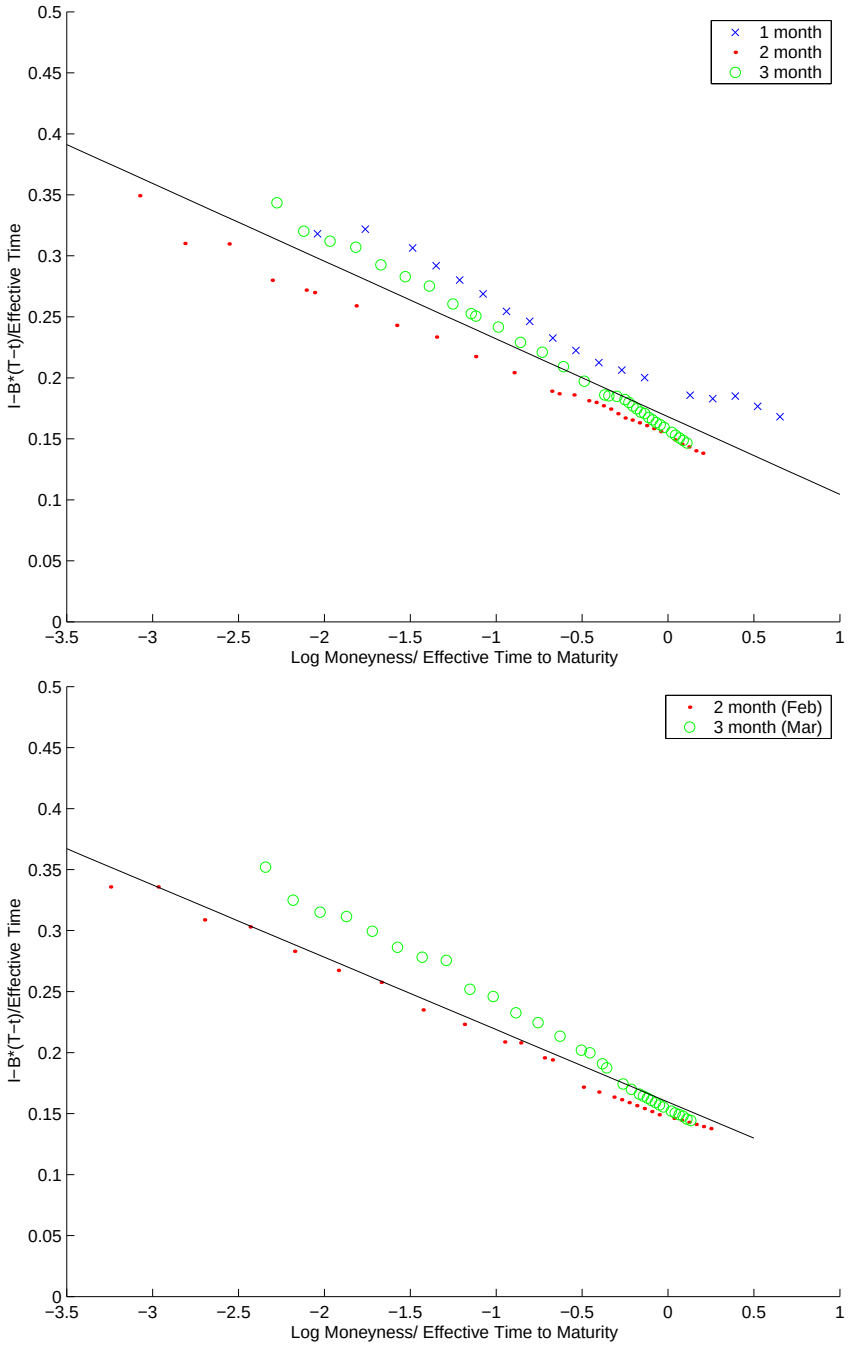

Figure 11: *Maturity-adjusted implied volatility as a function of log-moneyness to ETM on the last day before the shortest dated options disappear (January 18, 2000, top) and after (January 19, 2000, bottom) . Notice the strands for each maturity are tighter than with the regular LMMR fit in Figure 4.*

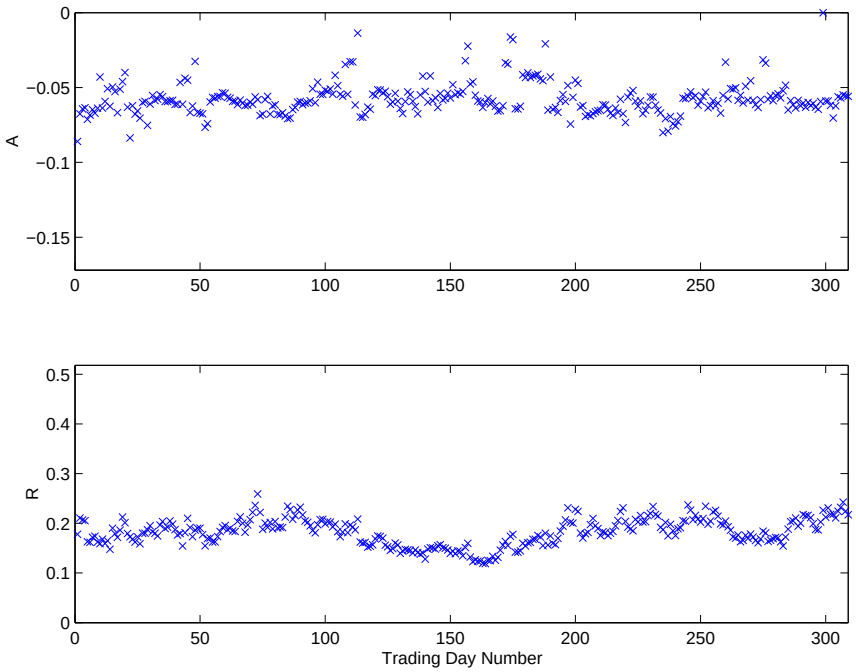

Figure 12: *Daily fitted slope A & residual R for options with at least 2 and at most 93 days to maturity fit to ETM formula. Statistics: Mean $(A) = -0.0577$, Std $(A) = 0.0107$; Mean $(R) = 0.1827$, Std $(R) = 0.0271$.*

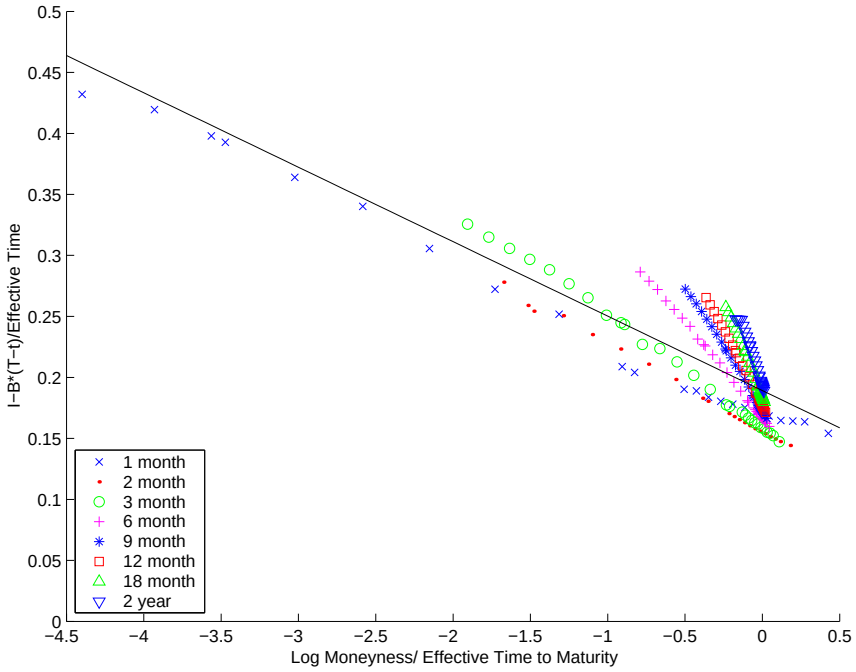

Figure 13: *ETM fit to all maturities (including 6 month, 9 month, 1, 1.5 and 2 year options) on January 14, 2000. Notice the diverging strands for the longer maturities.*

We conjecture that inclusion of a second slower (mean-reverting) factor in the volatility dynamics (as discussed in Section 1.2 and [4]) will help with these longer maturities. Figure 13 suggests that the implied volatility skews of longer maturity options are less sensitive to maturity than those of the shorter options (compare the relative closeness of the two-year skew to the one-year skew against the gap between the three- and six-month skews). We can also see this indirectly in Figure 6, where the fitted LMMR slope $a_{(t,T)}$ wants to dull the $(T-t)^{-1}$ predicted behaviour of the term-structure at small maturities. In a work in preparation, we study the empirical performance of a two-factor stochastic volatility model with a fast and a slow factor.

References

[1] Y. Aït-Sahalia and A. Lo. Nonparametric esimation of state-price densities implicit in financial asset prices. *J. Finance*, 53(2), April 1998.

[2] S. Alizadeh, M. Brandt, and F. Diebold. Range-based estimation of stochastic volatility models. *Journal of Finance*, 57(3):1047–91, 2002.

[3] T. Andersen and T. Bollerslev. Intraday periodicity and volatility persistence in financial markets. *J. Empirical Finance*, 4:115–158, 1997.

[4] J.-P. Fouque, G. Papanicolaou, K. R. Sircar, and K. Solna. Short Time-Scale in S&P 500 Volatility. *Journal of Computational Finance*, 2002. To appear.

[5] J.-P. Fouque, G. Papanicolaou, K. R. Sircar, and K. Solna. Singular perturbations in option pricing. *Preprint*, 2002.

[6] J.-P. Fouque, G. Papanicolaou, and K.R. Sircar. *Derivatives in Financial Markets with Stochastic Volatility*. Cambridge University Press, 2000.

[7] J. Hull and A. White. The Pricing of Options on Assets with Stochastic Volatilities. *J. Finance*, XLII(2):281–300, June 1987.

[8] S. Kou. A jump diffusion model for option pricing with three properties: leptokurtic feature, volatility smile, and analytical tractability. *Preprint*, 1999.

[9] D. Madan, P. Carr, and E. Chang. The variance gamma process and option pricing. *European Finance Review*, 2(1):79–105, 1999.

[10] G. Willard. *Calculating prices and sensitivities for path-independent derivative securities in multifactor models*. PhD thesis, Washington University in St. Louis, October 1996.